

Atmospheric correction of satellite ocean color imagery: the black pixel assumption

David A. Siegel, Menghua Wang, Stéphane Maritorena, and Wayne Robinson

The assumption that values of water-leaving radiance in the near-infrared (NIR) are negligible enable aerosol radiative properties to be easily determined in the correction of satellite ocean color imagery. This is referred to as the black pixel assumption. We examine the implications of the black pixel assumption using a simple bio-optical model for the NIR water-leaving reflectance $[\rho_w(\lambda_{\text{NIR}})]_N$. In productive waters [chlorophyll (Chl) concentration $>2 \text{ mg m}^{-3}$], estimates of $[\rho_w(\lambda_{\text{NIR}})]_N$ are several orders of magnitude larger than those expected for pure seawater. These large values of $[\rho_w(\lambda_{\text{NIR}})]_N$ result in an overcorrection of atmospheric effects for retrievals of water-leaving reflectance that are most pronounced in the violet and blue spectral region. The overcorrection increases dramatically with Chl, reducing the true water-leaving radiance by roughly 75% when Chl is equal to 5 mg m^{-3} . Relaxing the black pixel assumption in the correction of Sea-Viewing Wide Field-of-View Sensor (SeaWiFS) satellite ocean color imagery provides significant improvements in Chl and water-leaving reflectance retrievals when Chl values are greater than 2 mg m^{-3} . Improvements in the present modeling of $[\rho_w(\lambda_{\text{NIR}})]_N$ are considered, particularly for turbid coastal waters. However, this research shows that the effects of nonzero NIR reflectance must be included in the correction of satellite ocean color imagery. © 2000 Optical Society of America

OCIS codes: 010.0010, 280.0280, 010.4450.

1. Introduction

It is well recognized that more than 90% of the signal measured by an ocean color satellite sensor is due to the confounding influence of the atmosphere. The atmospheric and ocean surface effects must be removed before ocean radiance signals can be analyzed for the purposes of understanding the ocean biosphere. This step in the processing of satellite ocean color imagery is referred to as the atmospheric correction procedure.¹ Typically, the satellite-sensed radiance $L_t(\lambda)$ —or, equivalently, reflectance $\rho_t(\lambda)$ ($=\pi L_t(\lambda)/[F_0(\lambda)\mu_0]$ where $F_0(\lambda)$ is the extraterrestrial

solar irradiance and μ_0 is the cosine of the solar zenith angle)—is partitioned into components corresponding to distinct physical processes, or

$$\rho_t(\lambda) = \rho_r(\lambda) + \rho_a(\lambda) + \rho_{ra}(\lambda) + T(\lambda)\rho_g(\lambda) + t(\lambda)\rho_{wc}(\lambda) + t(\lambda)\rho_w(\lambda). \quad (1)$$

The first three terms on the right-hand side of Eq. (1) represent the contributions from atmospheric scattering that are due to air molecules (Rayleigh), aerosols, and Rayleigh–aerosol interactions, respectively. The terms $T(\lambda)$ and $t(\lambda)$ are the direct and diffuse transmittances of the atmospheric column, respectively; $\rho_g(\lambda)$ represents the effects of Sun glitter off the sea surface; $\rho_{wc}(\lambda)$ is the reflectance of ocean whitecaps; and $\rho_w(\lambda)$ is the water-leaving reflectance, the desired quantity in ocean color remote sensing.^{1,2} In Eq. (1), the Rayleigh scattering term $\rho_r(\lambda)$ and transmittances $T(\lambda)$ and $t(\lambda)$ can be calculated accurately,^{3–6} the ocean whitecap contributions can be estimated with the surface wind speed,^{7–9} and Sun-glitter-contaminated observations are generally avoided. This leaves the contributions from scattering by aerosols and Rayleigh–aerosol interactions, $\rho_a(\lambda) + \rho_{ra}(\lambda)$, and the ocean, $\rho_w(\lambda)$, as unknowns to be determined. To solve for these terms, it is first assumed that the near-infrared (NIR) water-leaving

D. A. Siegel (davey@icess.ucsb.edu) and S. Maritorena are with the Institute for Computational Earth System Science, University of California, Santa Barbara, Santa Barbara, California 93106-3060. D. A. Siegel is also with the Department of Geography and the Donald Bren School of Environmental Science and Management at the University of California, Santa Barbara. M. Wang is with the University of Maryland Baltimore County, NASA Goddard Space Flight Center, Code 970.2, Greenbelt, Maryland 20771. W. Robinson is with SAIC General Sciences Corporation, NASA Goddard Space Flight Center, Greenbelt, Maryland 20771.

Received 15 September 1999; revised manuscript received 4 May 2000.

0003-6935/00/213582-10\$15.00/0

© 2000 Optical Society of America

radiance is negligible, enabling estimates of NIR aerosol-scattering terms to be made. Values of $\rho_a(\lambda) + \rho_{ra}(\lambda)$ for the visible bands are arrived at by the extrapolation of the NIR aerosol signals into the visible by use of appropriate aerosol models.² The assumption that the NIR ocean is optically black [$\rho_w(\lambda_{\text{NIR}}) = 0$] was initially made for clear ocean waters¹⁰ and is referred to as the black pixel assumption.

To relate the derived water-leaving reflectance to the inherent optical properties of the ocean, all geometric influences on $\rho_w(\lambda)$ must be eliminated, which can be accomplished when the water-leaving reflectance $[\rho_w(\lambda)]_N$ is normalized to a zenith sky similar to the definition of the normalized water-leaving radiance $[L_w(\lambda)]_N$ ¹⁰:

$$[L_w(\lambda)]_N = L_w(\lambda) / \mu_0 t_0(\lambda), \quad (2)$$

$$[\rho_w(\lambda)]_N = \frac{\pi [L_w(\lambda)]_N}{F_0(\lambda)} \equiv \frac{\rho_w(\lambda)}{t_0(\lambda)}, \quad (3)$$

where $t_0(\lambda)$ is the atmospheric diffuse transmittance in the solar direction. Ocean constituent concentrations are determined from estimates of $[\rho_w(\lambda)]_N$ by use of either empirical^{11,12} or semianalytical^{13–15} models.

The Sea-Viewing Wide Field-of-View Sensor (SeaWiFS) has provided the oceanographic community an unprecedented opportunity to assess globally the ocean biological and biogeochemical processes.¹⁶ SeaWiFS imagery is available with a spatial resolution of 1.1 km (at nadir) and a sampling schedule of nearly once per day. The SeaWiFS atmospheric correction procedure assumes that bands 7 and 8 (centered at 765 and 865 nm, respectively) are black pixels and are used to estimate aerosol radiance levels and to select appropriate aerosol optical models.² For the open ocean conditions, the atmospheric correction algorithm is thought to be accurate to within ~5%.²

Unfortunately, the SeaWiFS determinations of water-leaving reflectance in the violet and blue (SeaWiFS bands 1 and 2) underestimate dramatically *in situ* observations for highly productive waters [i.e., low $[\rho_w(\lambda)]_N$ retrievals]. This can be seen in a comparison of nearly simultaneous match-ups of SeaWiFS and field observations of $[\rho_w(\lambda)]_N$ at 412, 443, and 490 nm and chlorophyll (Chl) concentration (Fig. 1) provided from the Sensor Intercomparison and Merger for Biological and Interdisciplinary Oceanic Studies (SIMBIOS) project. Details of the procedures used in developing these satellite and field data comparisons can be found in Ref. 17. Obviously, the present version of SeaWiFS processing (version 2) underestimates determinations of $[\rho_w(412)]_N$ when values of $[\rho_w(412)]_N$ are small [less than 0.005; Fig. 1(a)]. A similar, though less pronounced, underestimation is found for $[\rho_w(443)]_N$ [Fig. 1(b)]. However, the comparison of the field and satellite Chl is good with no real bias from the one-to-one line [Fig.

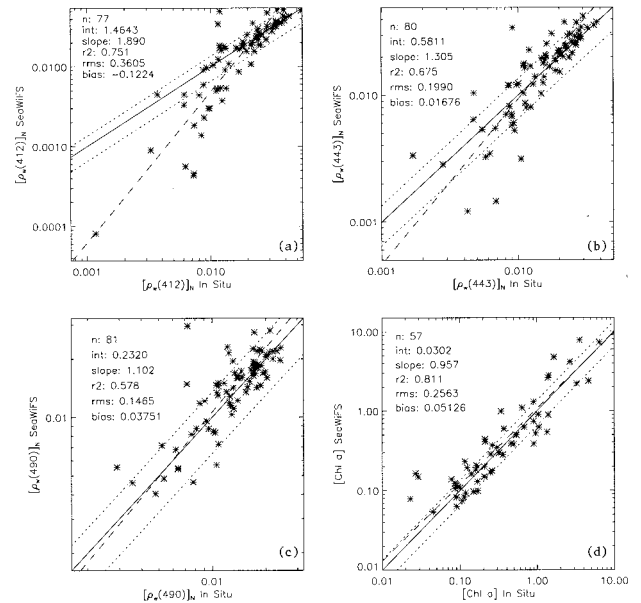


Fig. 1. SIMBIOS *in situ* and SeaWiFS imagery match-up comparison for $[\rho_w(\lambda)]_N$ at 412, 443, 490, and Chl. The SeaWiFS observations are processed with the standard version 2 processing procedures. Procedures explaining the match-up data set procedure are provided in Ref. 17.

1(d)]. In general, SeaWiFS provides excellent Chl retrievals, explaining 81% of the observed variance.

Several factors may be responsible for poor performance of the SeaWiFS atmospheric correction procedure. However, the overcorrection for $[\rho_w(\lambda)]_N$ retrievals is most apparent for low values of $[\rho_w(412)]_N$ when Chl observations are large. This suggests that this problem may be due to the ocean itself. We hypothesize that the inappropriate application of the black pixel assumption is responsible for some of the problems highlighted in Fig. 1. This was first suggested by Arnone and colleagues,¹⁸ and other researchers have worked on this issue as well.^{19,20} Here we study the implications of the black pixel assumption on the correction of satellite ocean color imagery. First, we develop a simple bio-optical algorithm for estimating $[\rho_w(\lambda_{\text{NIR}})]_N$ and quantify its magnitude using a recent ocean optics climatology.¹² We then theoretically evaluate the implications of relaxing the black pixel assumption on estimates of water-leaving radiance and provide an iterative correction scheme. Last, we demonstrate the implications of the black pixel assumption using SeaWiFS imagery.

2. Estimation of Ocean Contributions at the Near-Infrared Bands

Measurements of the water-leaving radiance spectrum have now become routine because of the need to calibrate and validate satellite ocean color imagery. However, to the best of our knowledge, no direct estimates of $[\rho_w(\lambda_{\text{NIR}})]_N$ are available because of the extreme difficulty in making upwelling NIR radiance measurements. Hence, values for $[\rho_w(\lambda_{\text{NIR}})]_N$ are

Table 1. Parameters used to Determine $[\rho_w(\lambda_{\text{NIR}})]_N$

Parameter	Center Wavelength (nm)			Reference
	670 (6) ^a	760 (7) ^a	865 (8) ^a	
$a_w(\lambda)$ (m ⁻¹)	0.4346	2.550	4.286	Ref. 23 for bands 6 and 7 Ref. 22 for band 8
$b_{\text{bw}}(\lambda)$ (m ⁻¹)	0.00041	0.00024	0.00014	Ref. 23
$F_0(\lambda)$ (μW cm ⁻² nm ⁻¹)	153.41	122.24	98.82	Ref. 29

^aSeaWiFS band number.

estimated most expediently by use of optical models and knowledge of NIR inherent optical properties.

Values of $[\rho_w(\lambda)]_N$ can be modeled as a function of the spectral absorption $[a(\lambda)]$ and backscattering $[b_b(\lambda)]$ coefficients,¹³ or

$$[\rho_w(\lambda)]_N = \pi(t/n)^2 \sum_{i=1}^2 g_i \left[\frac{b_b(\lambda)}{b_b(\lambda) + a(\lambda)} \right]^i, \quad (4)$$

where $(t/n)^2$ accounts for the transmission of upwelling radiance and downwelling irradiance across the sea surface²¹ and the constants g_1 and g_2 are 0.0949 and 0.0794 sr⁻¹, respectively.¹³

Absorption of NIR radiation by seawater dominates over other factors, enabling $a(\lambda_{\text{NIR}})$ to be modeled with its pure-water value $a_w(\lambda_{\text{NIR}})$.^{22,23} For the case in which bands in the red spectral region are required for an atmospheric correction scheme, an accounting of particulate-induced absorption is required.²⁴ On the other hand, the modeling of the backscattering coefficient is problematic as values of $b_b(\lambda_{\text{NIR}})$ that are due to particulates are much larger than those that are due to seawater.^{15,25} Hence a predictive knowledge of the particulate backscattering coefficient $b_{\text{bp}}(\lambda_{\text{NIR}})$ is required. Provided with a model for $b_{\text{bp}}(\lambda_{\text{NIR}})$, estimates of NIR-normalized water-leaving reflectance can be expressed as

$$[\rho_w(\lambda_{\text{NIR}})]_N \cong \pi(t/n)^2 \times \sum_{i=1}^2 g_i \left[\frac{b_{\text{bp}}(\lambda_{\text{NIR}}) + b_{\text{bw}}(\lambda_{\text{NIR}})}{b_{\text{bp}}(\lambda_{\text{NIR}}) + b_{\text{bw}}(\lambda_{\text{NIR}}) + a_w(\lambda_{\text{NIR}})} \right]^i, \quad (5)$$

where the necessary parameters are presented in Table 1.

We compare two basic approaches for determining $b_{\text{bp}}(\lambda_{\text{NIR}})$. The first uses estimates of the chlorophyll a concentration to determine $b_{\text{bp}}(\lambda_{\text{NIR}})$ ^{11,26} whereas the second uses determinations of water-leaving radiance and the assumption of optical closure.¹⁵ Both relationships are empirical and were derived from field data within the visible spectral region and extrapolated into the NIR.

The bio-optical modeling of $b_{\text{bp}}(\lambda_{\text{NIR}})$ assumes that its variability is driven by the chlorophyll content of the water, or

$$b_{\text{bpBO}}(\lambda_{\text{NIR}}) = 0.416 \text{ Chl}^{0.766} (0.002 + (550/\lambda_{\text{NIR}}) \times \{0.02[0.5 - 0.25 \log_{10}(\text{Chl})]\}), \quad (6)$$

where Chl is the chlorophyll concentration (in mg m⁻³) and λ_{NIR} is the center NIR wavelength of interest. The term outside the parentheses on the right-hand side of Eq. (6) gives the particulate scattering coefficient at 550 as recently updated,²⁷ whereas the term within parentheses models the spectral dependence and the magnitude of the backscattered fraction.²⁶ This formulation assumes that the spectral dependence for $b_{\text{bpBO}}(\lambda_{\text{NIR}})$ goes as λ^{-1} throughout the entire spectral range. Similar bio-optical algorithms are available,^{13,26} all of which give broadly similar results {within a factor of 4 for $[\rho_w(\lambda_{\text{NIR}})]_N$; comparison not shown}.

The optical closure backscatter model $b_{\text{bpOC}}(\lambda_{\text{NIR}})$ is derived from reflectance-based estimates of $b_{\text{bp}}(\lambda)$.¹⁵ This parameterization assumes that the magnitude of spectral backscatter is a linear function of the water-leaving reflectance at 551 nm, $[\rho_w(551)]_N$, whereas the spectral slope of particulate backscatter is a function of the ratio of $[\rho_w(443)]_N$ to $[\rho_w(488)]_N$, or

$$b_{\text{bpOC}}(\lambda_{\text{NIR}}) = \{X_0 + X_1[\rho_w(551)]_N\} \times \left(\frac{551}{\lambda_{\text{NIR}}} \right)^{Y_0 + Y_1[\rho_w(443)]_N/[\rho_w(488)]_N}, \quad (7)$$

where $X_0 = -0.00182$, $X_1 = 0.655$, $Y_0 = -1.13$, and $Y_1 = 2.57$.¹⁵ The ratio of $[\rho_w(443)]_N$ to $[\rho_w(488)]_N$ is large in blue waters and small in green and turbid waters, causing the spectral slope for $b_{\text{bpOC}}(\lambda_{\text{NIR}})$ to vary from 0 for turbid waters to greater than 2 for clear, oligotrophic waters. The magnitude of $b_{\text{bpOC}}(\lambda_{\text{NIR}})$ is controlled by $[\rho_w(551)]_N$ where, to first order, backscattering regulates ocean color variability.¹¹

The two estimates of $b_{\text{bp}}(\lambda)$ are plotted against Chl in Fig. 2(a) for $b_{\text{bp}}(550)$ and in Fig. 2(b) for $b_{\text{bp}}(865)$ for the SeaBAM (SeaWiFS Bio-optical Algorithm Mini-workshop) data set.¹² Values of $b_{\text{bp}}(550)$ are comparable to the pure-water values [the dotted line in Fig. 2(a)], whereas estimates of $b_{\text{bp}}(865)$ are often a factor of 10 greater than $b_{\text{bw}}(865)$. Compared with the bio-optical determinations of $b_{\text{bp}}(550)$ and $b_{\text{bp}}(865)$, the closure-based estimates are a weaker function of Chl, particularly at 550 nm. Mean values of $b_{\text{bp}}(550)$, $b_{\text{bp}}(760)$, and $b_{\text{bp}}(865)$ are similar for both methods (Table 2).

Scale estimates for $[\rho_w(\lambda_{\text{NIR}})]_N$ can be made by use of both methods to determine $b_{\text{bp}}(\lambda_{\text{NIR}})$ [Figs.

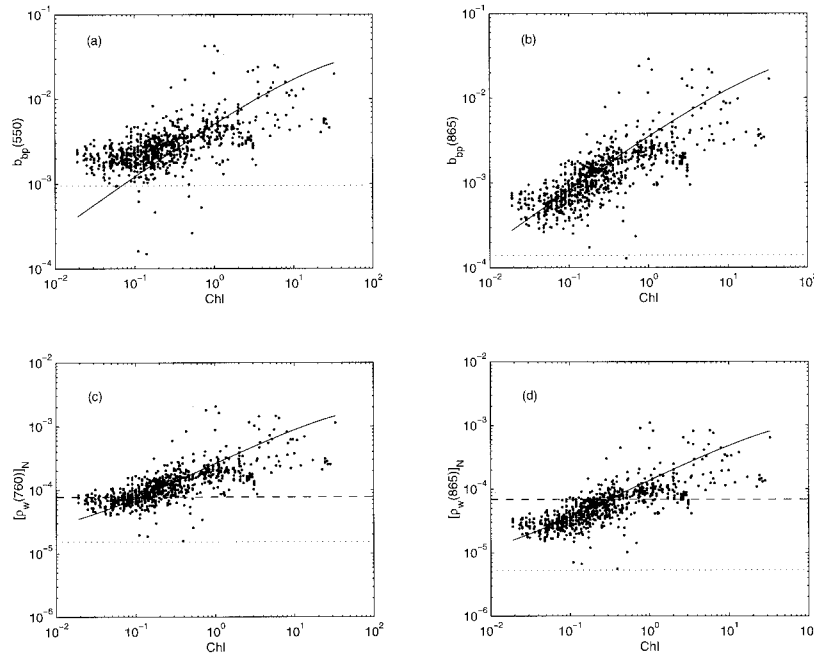


Fig. 2. Comparison of $b_{bp}(\lambda)$ and $[\rho_w(\lambda_{NIR})]_N$ estimates versus Chl by use of the SeaBAM data set¹² for (a) $b_{bp}(550)$, (b) $b_{bp}(865)$, (c) $[\rho_w(760)]_N$, and (d) $[\rho_w(865)]_N$. The results of the bio-optical algorithm [Eq. (6)] are shown as the solid curve, whereas the points are from the closure model [Eq. (7)]. The dotted horizontal lines in (c) and (d) are estimates of $[\rho_w(\lambda_{NIR})]_N$ assuming that $b_{bp}(\lambda_{NIR})$ equals zero (the clear-water reflectance). The dashed horizontal lines in (c) and (d) are the one digital count level for the SeaWiFS instrument for bands 7 and 8.²⁸

2(c) and 2(d)]. As expected, an increasing trend in $[\rho_w(\lambda_{NIR})]_N$ is found with increasing Chl where values of $[\rho_w(865)]_N$ increase from $\sim 10^{-5}$ for $\text{Chl} \leq 0.5 \text{ mg m}^{-3}$ to nearly 10^{-3} for $\text{Chl} > 10 \text{ mg m}^{-3}$. Both estimates of $[\rho_w(\lambda_{NIR})]_N$ are much greater than expected for pure seawater [where $b_{bp}(\lambda_{NIR}) = 0$ and $\alpha(\lambda_{NIR}) = \alpha_w(\lambda_{NIR})$; the dotted lines in Figs. 2(c) and 2(d)]. Estimates of $[\rho_w(\lambda_{NIR})]_N$ found by use of the bio-optical $b_{bp}(\lambda)$ algorithm are similar to the optical closure model, although a large degree of scatter is observed among these estimates of $[\rho_w(\lambda_{NIR})]_N$ [Figs. 2(c) and 2(d); Table 3].

The importance of the black pixel assumption to SeaWiFS imagery can be evaluated by a comparison of the present estimates of $[\rho_w(\lambda_{NIR})]_N$ to the single digital count sensed by the SeaWiFS instrument.²⁸ Estimates of $[\rho_w(\lambda_{NIR})]_N$ are greater than the SeaWiFS one digital count level [the dashed lines in Figs. 2(c) and 2(d)] for $\text{Chl} > \sim 0.5 \text{ mg m}^{-3}$. Hence NIR water-leaving radiance may be important for the atmospheric correction of SeaWiFS imagery in moderate to highly productive waters.

The choice of the appropriate $[\rho_w(\lambda_{NIR})]_N$ param-

eterization is not straightforward as there are few direct observations of backscatter that can be used to develop or validate a parameterization. The bio-optical approach has been applied extensively within the ocean optics community^{11,24,26} whereas the closure model has been introduced recently and has not been validated independently.¹⁵ Both $b_{bp}(\lambda_{NIR})$ models have extensive uncertainties that feed into the modeling of $[\rho_w(\lambda_{NIR})]_N$. For present purposes, we use the bio-optical approach simply because it is the known quantity of the two candidates. It is likely that future implementations of a black pixel correction procedure will use approaches similar to the closure model, especially for turbid, coastal, and inland waters (see Section 5 for further discussion).

3. Effects of the Black Pixel Assumption on the SeaWiFS Atmospheric Correction Algorithm

A. Errors in $[\rho_w(\lambda)]_N$ Retrievals

We address the importance of the black pixel assumption and its effect on $[\rho_w(\lambda)]_N$ retrievals using the present version of the SeaWiFS atmospheric correc-

Table 2. Ensemble Mean and Standard Deviation (in parentheses) Estimates for $b_{bp}(550)$, $b_{bp}(760)$, and $b_{bp}(865)$ by use of SeaBAM ($N = 919$)

Model	$b_{bp}(550) \text{ (m}^{-1}\text{)}$	$b_{bp}(760) \text{ (m}^{-1}\text{)}$	$b_{bp}(865) \text{ (m}^{-1}\text{)}$
Bio-optical [Eq. (6)]	0.00322 (0.00358)	0.00250 (0.00290)	0.00227 (0.00268)
Closure [Eq. (7)]	0.00336 (0.00328)	0.00208 (0.00261)	0.00174 (0.00239)

Table 3. Ensemble Mean and Standard Deviation (in parentheses) Estimates for $[\rho_w(670)]_N$, $[\rho_w(760)]_N$, and $[\rho_w(865)]_N$ by use of SeaBAM ($N = 919$)

Model	$[\rho_w(670)]_N (\times 10^3)$	$[\rho_w(760)]_N (\times 10^3)$	$[\rho_w(865)]_N (\times 10^3)$
Bio-Optical [Eq. (6)]	1.085 (0.875)	0.174 (0.184)	0.091 (0.101)
Closure [Eq. (7)]	1.027 (0.937)	0.148 (0.166)	0.071 (0.091)

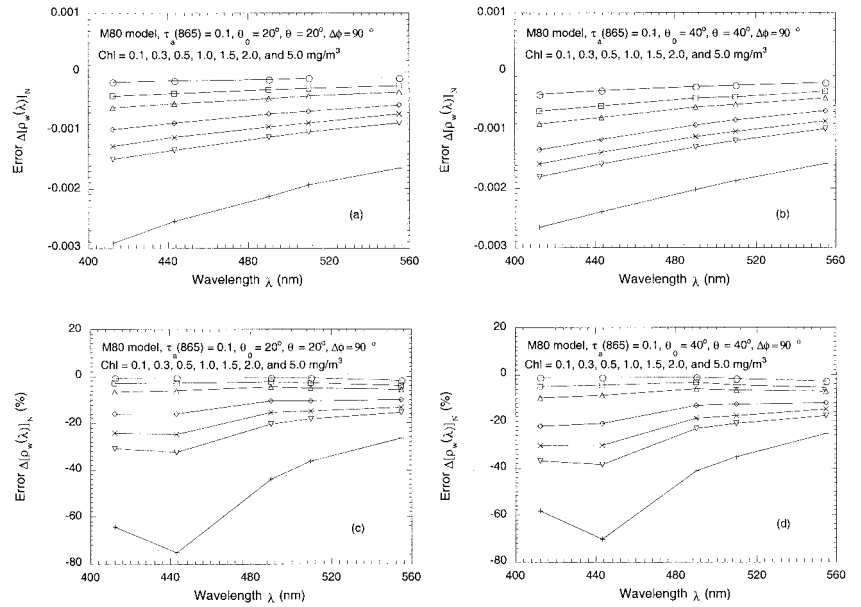


Fig. 3. Errors $\Delta[\rho_w(\lambda)]_N$ in the retrieved $[\rho_w(\lambda)]_N$ by our ignoring the NIR ocean contributions for the SeaWiFS bands 1–5 for the aerosol M80 model with an optical thickness of 0.1 at 865 nm, seven Chl values, and for the solar and viewing geometries of (a) and (c) $\theta_0 = 20^\circ$, $\theta = 20^\circ$, $\Delta\phi = 90^\circ$ and (b) and (d) $\theta_0 = 40^\circ$, $\theta = 40^\circ$, $\Delta\phi = 90^\circ$. Note that (c) and (d) are in relative errors (%). The curves from the top to the bottom in these figures correspond to Chl concentrations of 0.1, 0.3, 0.5, 1.0, 1.5, 2.0, and 5.0 mg m^{-3} , respectively.

tion algorithm² with a maritime aerosol model, a relative humidity of 80% (M80), and an aerosol optical thickness at 865 nm of 0.1. We compare retrievals using a fully black ocean $\{[\rho_w(\lambda)]_N = 0 \text{ for all } \lambda\}$ with those made for an ocean that is black in the visible $\{[\rho_w(\lambda)]_N = 0 \text{ for } 400 < \lambda < 700 \text{ nm}\}$ but which reflectance in the NIR, $[\rho_w(\lambda_{\text{NIR}})]_N$, is a known function of Chl [given by relation (5) and Eq. (6)]. The assumed water-leaving signals are used in the calculation of the top of the atmosphere reflectance spectra from which $[\rho_w(\lambda)]_N$ are then computed and corrected for inherent noise (~ 0.001 in reflectance units^{1,2,29}). The difference between retrieved $[\rho_w(\lambda)]_N$ for the fully black ocean and for the nonzero NIR ocean $\Delta[\rho_w(\lambda)]_N$ quantifies the importance of the black pixel assumption.

Estimates of $\Delta[\rho_w(\lambda)]_N$ illustrate the effects of varying the NIR water reflectance on retrievals of $[\rho_w(\lambda)]_N$ (Fig. 3). In these depictions, two solar and viewing geometries [$\theta_0 = 20^\circ$, $\theta = 20^\circ$, $\Delta\phi = 90^\circ$ in Figs. 3(a) and 3(c) and $\theta_0 = 40^\circ$, $\theta = 40^\circ$, $\Delta\phi = 90^\circ$ in Figs. 3(b) and 3(d)] are shown. The magnitude of the error term $\Delta[\rho_w(\lambda)]_N$ is shown in Figs. 3(a) and 3(b), and normalized error estimates are given in Figs. 3(c) and 3(d) where the bio-optical model of Ref. 13 is employed. Similar results were obtained for other aerosol models, aerosol optical thicknesses, and solar and viewing geometries (results not shown).

In general, values of $\Delta[\rho_w(\lambda)]_N$ increase dramatically with Chl, and this effect is more accentuated for the blue wave bands (Fig. 3). When the NIR ocean contributions are ignored, this leads to an overcorrection of aerosol reflectance. The effects become important $\{>10\%$ of the retrieved $[\rho_w(\lambda)]_N\}$ for Chl $> 0.5 \text{ mg m}^{-3}$. Hence, for oligotrophic conditions, existing SeaWiFS correction algorithms should perform well. However, errors will be large for ocean regions with high chlorophyll concentrations.

B. Errors in Two-Band Ratio Chlorophyll Retrievals

Many algorithms for determining ocean chlorophyll concentrations use ratios of normalized water-leaving reflectance.^{11,12} For example, the OC2v2 chlorophyll algorithm uses the ratio of SeaWiFS bands 3 and 5 $\{R(3,5) = [\rho_w(490)]_N / [\rho_w(555)]_N\}$ in a polynomial relationship.³⁰ We quantify the error that is due to the black pixel assumption for any arbitrary band ratio $\Delta R(i, j)$ as

$$\Delta R(i, j) = \frac{[\rho_w(\lambda_i)]_N + \Delta[\rho_w(\lambda_i)]_N}{[\rho_w(\lambda_j)]_N + \Delta[\rho_w(\lambda_j)]_N} - \frac{[\rho_w(\lambda_i)]_N}{[\rho_w(\lambda_j)]_N}, \quad (8)$$

where i and j are the SeaWiFS band numbers. Determinations of $\Delta R(i, j)$ are made by use of the previous calculations of $\Delta[\rho_w(\lambda)]_N$ and values of $[\rho_w(\lambda)]_N$ estimated from the semianalytical algorithm of Ref. 13. Typical errors in the retrieved ratio values between SeaWiFS bands 2 and 5, $R(2,5)$, and bands 3 and 5, $R(3,5)$, are shown in Table 4. As before, the M80 aerosol model with an aerosol optical thickness of 0.1 at 865 nm and the two solar and viewing geometries are used. The present results show that for Chl less than 1 mg m^{-3} , differences that are due to the application of a NIR correction are small ($\leq 2\%$). However, for Chl greater than 2 mg m^{-3} , band ratio errors increase dramatically (Table 4). Errors are greater than 20% for $R(3,5)$ and more than 60% for $R(2,5)$ for a Chl of 5 mg m^{-3} . Band ratio errors are greater for $R(2,5)$ than for $R(3,5)$ as expected.

We compare the effects of the black pixel assumption using the present version of the SeaWiFS algorithm and a polynomial band ratio algorithm using $R(2,5)$ (Morel-3 algorithm in Ref. 12). For low Chl waters (Chl $< 0.5 \text{ mg m}^{-3}$), the errors in chlorophyll retrievals are not large ($< 5\%$; Table 5). However for Chl $> 2 \text{ mg m}^{-3}$, the errors can be greater than 100%.

Table 4. Error $\Delta R(i, j)$ (in percent) in the Retrieved Ratio of the Normalized Water-Leaving Reflectance between the SeaWiFS Bands 2 and 5 and bands 3 and 5^a

Chl (mg/m ⁻³)	$\theta_0 = 20^\circ, \theta = 20^\circ, \Delta\phi = 90^\circ$		$\theta_0 = 40^\circ, \theta = 40^\circ, \Delta\phi = 90^\circ$	
	$\Delta R(2,5)$	$\Delta R(3,5)$	$\Delta R(2,5)$	$\Delta R(3,5)$
0.1	1.13	1.02	2.05	1.89
0.3	0.96	1.43	0.90	1.83
0.5	-0.51	1.17	-1.55	1.21
1.0	-6.49	-0.58	-9.98	-1.37
1.5	-13.56	-3.00	-18.02	-4.19
2.0	-20.22	-5.45	-25.63	-7.05
5.0	-66.27	-23.56	-60.48	-21.63

^aCalculations were determined with the M80 aerosol model with $\tau_a(865) = 0.1$ and various chlorophyll concentrations and the two solar and viewing geometries.

For high Chl conditions, the errors that are due to the NIR ocean contribution are greater for the Morel-3 algorithm than for the OC2v2 algorithm as the Morel-3 relationship uses the $R(2,5)$ ratio (Table 5). We conclude that the NIR ocean contribution must be included in the atmospheric correction schemes for moderate to high Chl conditions.

C. Accounting for $[\rho_w(\lambda_{\text{NIR}})]_N$ in the SeaWiFS Atmospheric Correction Procedure

The accounting of $[\rho_w(\lambda_{\text{NIR}})]_N$ in atmospheric correction requires an iterative approach. The iterative procedure entails an initial guess for Chl, an estimate for $[\rho_w(\lambda_{\text{NIR}})]_N$ and its removal from the reflectance budget [Eq. (1)], and application of the existing SeaWiFS atmospheric correction algorithm to retrieve a new Chl. This process is repeated until a converged Chl value is obtained. The NIR correction procedure can be summarized schematically as follows:

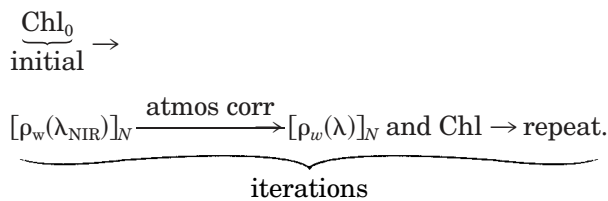


Table 5. Error in the Retrieved Chlorophyll Concentration (in percent) by use of the Morel-3 and OC2v2 Algorithms^a

Chl (mg/m ⁻³)	$\theta_0 = 20^\circ, \theta = 20^\circ, \Delta\phi = 90^\circ$		$\theta_0 = 40^\circ, \theta = 40^\circ, \Delta\phi = 90^\circ$	
	Morel-3	OC2v2	Morel-3	OC2v2
0.1	-2.0	-2.8	-3.7	-5.1
0.3	-1.5	-3.3	-1.4	-4.2
0.5	0.8	-2.7	2.6	-2.7
1.0	12.0	1.3	18.4	3.15
1.5	26.9	7.0	35.8	9.8
2.0	42.2	12.9	53.4	16.7
5.0	158.2	58.2	144.4	53.4

^aThe atmosphere is specified as an M80 aerosol type with $\tau_a(865) = 0.1$. Various true chlorophyll concentrations are used for two solar and viewing geometries.

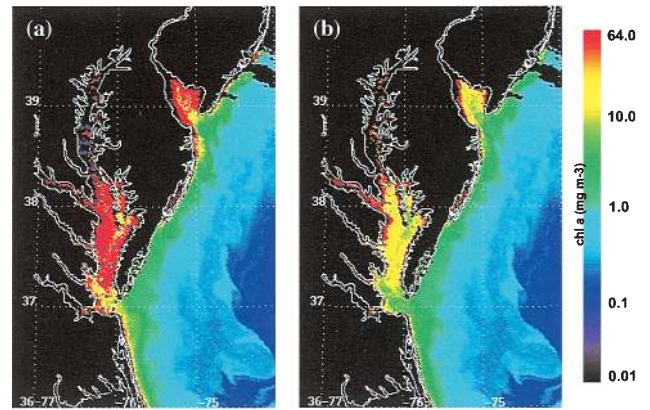


Fig. 4. SeaWiFS LAC chlorophyll scene for the Chesapeake Bay and adjacent waters from 19 May 1998 (S1998139171559, L1A_HNSG), processed with (a) the SeaWiFS standard processing (version 2) and (b) the present NIR correction procedure. The purple dots in (a) correspond to the location of field observations used in making Fig. 5(c).

The initial Chl value, Chl_0 , is set to 0.2 mg m^{-3} and iterations are stopped once the final Chl retrieval is within 20% of the last iterate. Typically, one (open ocean) to three (coastal waters) iterations are required. If the first iterated Chl value is less than 0.3 mg m^{-3} , the iterations are terminated.

4. Application to SeaWiFS Imagery

To assess the importance of the black pixel assumption, we apply the NIR correction scheme to SeaWiFS imagery on both local and global scales. First we use a SeaWiFS local-area coverage (LAC) image from the Chesapeake Bay region demonstrating that misapplication of the black pixel assumption leads to large errors in highly productive waters. Next we assess changes in the SIMBIOS global field and satellite match-up data set after correcting for $[\rho_w(\lambda_{\text{NIR}})]_N$. Last, we evaluate the effects of the black pixel assumption on global SeaWiFS imagery.

A. Example of SeaWiFS Imagery from the Chesapeake Bay

As discussed above, SeaWiFS chlorophyll retrievals often overestimate Chl values in productive waters (Fig. 1). A SeaWiFS LAC Chl image from 19 May 1998 for the Chesapeake Bay region (east coast of North America) is shown in Fig. 4(a). By use of the standard processing, most of the Chl retrievals throughout the bay are in excess of 64 mg m^{-3} , which is the maximum value quantified [Fig. 5(a)]. However, no field observations from this period show values in excess of 40 mg m^{-3} [Fig. 5(c)]. A reanalysis of this SeaWiFS image by use of the present NIR parameterization shows substantial improvements [Fig. 4(b)]. In particular, nearly all the excessive Chl retrievals ($>40 \text{ mg m}^{-3}$) were corrected, and the range of Chl retrievals is now consistent with the field observations [Figs. 5(b) and 5(c)].

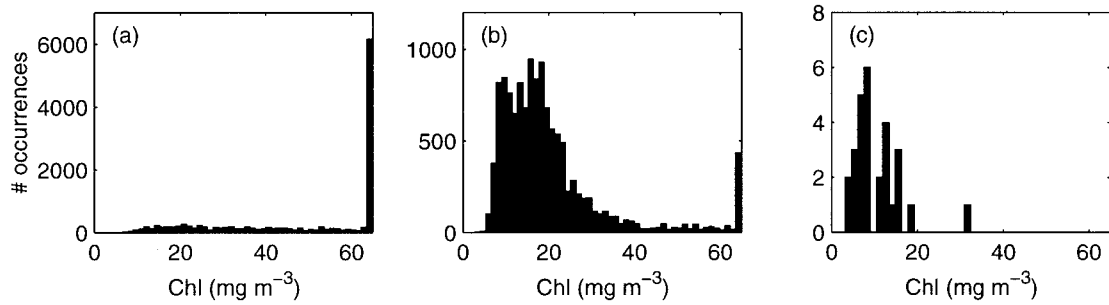


Fig. 5. Chlorophyll concentration histograms for observations taken from within the Chesapeake Bay from 19 May 1998 by use of (a) the SeaWiFS LAC scene and the standard processing (version 2), (b) the SeaWiFS LAC scene with the present NIR correction procedure, and (c) from *in situ* observations taken between 18 and 20 May 1998. The purple dots in Fig. 4(a) provide the location of the data used in making Fig. 5(c).

B. Global *In Situ* Match-Up Analyses

Despite the limited number of observations at high chlorophyll concentrations, the global match-up data set reprocessed with the present NIR algorithm shows improvements compared with the original analysis (Fig. 6). In particular, the regression slope between the two $[\rho_w(412)]_N$ retrievals is closer to one for the NIR-corrected data. Similarly, root mean square (rms) deviations between the satellite and the field observations are significantly less for the NIR-processed SeaWiFS retrievals for $[\rho_w(\lambda)]_N$ and Chl (Fig. 6).

Consistent with what can be seen with the example from the Chesapeake Bay (Figs. 4 and 5), there is a significant improvement in the correspondence between the SeaWiFS and the field estimates of Chl at high concentrations (Fig. 7). For $\text{Chl} > 1 \text{ mg m}^{-3}$, rms differences in Chl retrievals are smaller for the NIR processing (1.46 mg m^{-3}) than with the standard processing (2.04 mg m^{-3}).

C. Global Imagery Analysis

Analysis of global imagery enables the importance of the NIR correction to be put in context. Figure 8 shows frequency of occurrence distributions of the NIR error from two SeaWiFS Chl eight-day composite scenes (summer, 12–19 July 1998, and winter, 17–24 January 1998). The effects of the bio-optical NIR algorithm on global Chl retrievals are important ($>10\%$) only when the standard processing Chl is greater than 2 mg m^{-3} . These conditions occur for only 2.1 and 1.3% of the total number of good retrievals for the summer and winter composites, respectively. However, the effects of NIR water-leaving reflectance reach nearly 60% of the standard processing value (Fig. 8). The small ($<10\%$) normalized Chl errors found for $\text{Chl} < 0.02 \text{ mg m}^{-3}$ are due to the amplification of small round-off errors (which are an order of 0.001 mg m^{-3}) by the small normalization factor.

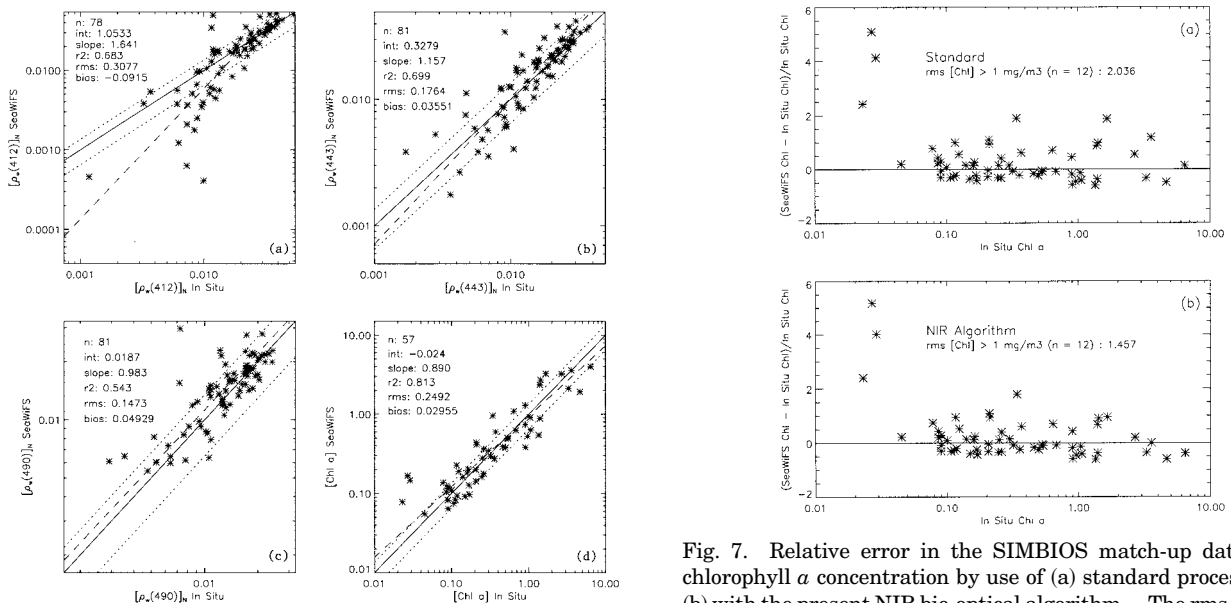


Fig. 6. SIMBIOS match-up data set for $[\rho_w(\lambda)]_N$ at 412, 443, 490, and Chl after the NIR correction procedure is performed. The format is identical to Fig. 1.

Fig. 7. Relative error in the SIMBIOS match-up data set for chlorophyll *a* concentration by use of (a) standard processing and (b) with the present NIR bio-optical algorithm. The rms deviation for high chlorophyll conditions ($\text{Chl} > 1 \text{ mg m}^{-3}$) decreases by a significant amount after the NIR correction is employed ($2.04\text{--}1.46 \text{ mg m}^{-3}$).

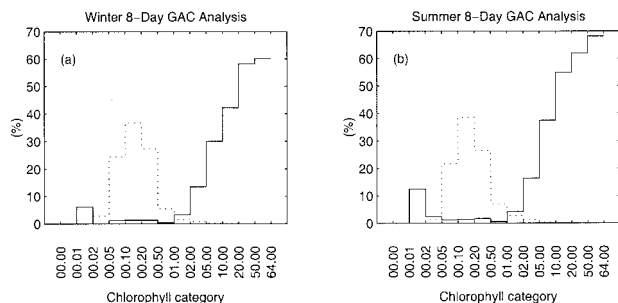


Fig. 8. Percentage reduction in SeaWiFS chlorophyll retrievals after implementation of the NIR correction procedure (solid line) as a function of the Chl retrieval from the standard processing. Data are shown for two 8-day composite SeaWiFS global-area coverage (GAC) scenes for (a) summer (12–19 July 1998) and (b) winter (17–24 January 1998) conditions. Also shown is the percentage occurrence of the different Chl intervals (dotted line).

The role of the black pixel assumption on retrievals of water-leaving reflectance can also be addressed (Fig. 9). As seen above, only for the highest Chl categories shown will the misapplication of the black pixel assumption have a large influence ($>20\%$) on the retrieved $[\rho_w(\lambda)]_N$ spectrum (Fig. 9). Significant effects ($\sim 10\%$) are also observed for the 1–2- mg m^{-3} category. Hence NIR water-leaving reflectance must be considered in the global processing of ocean color imagery.

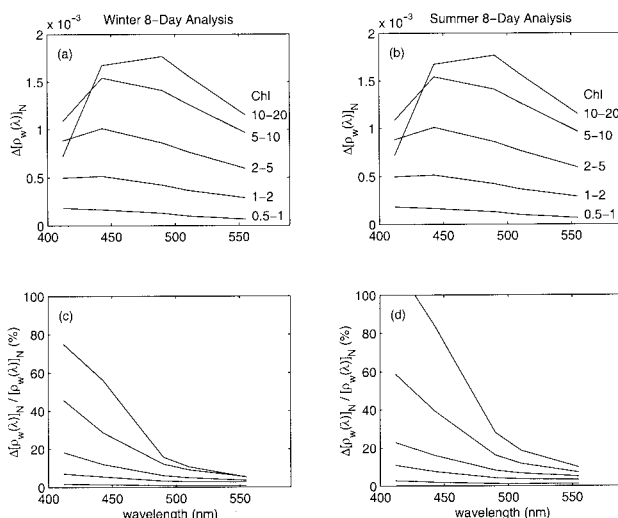


Fig. 9. Percentage improvement in water-leaving reflectance spectra retrievals (upper) and normalized to the estimated spectra (lower) after implementation of the NIR correction procedure (NIR corrected and standard). Data are shown for two 8-day composite SeaWiFS global-area coverage scenes for summer (right, 12–19 July 1998) and winter (left, 17–24 January 1998) conditions. The different curves correspond to categories of Chl concentrations of 10–20, 5–10, 2–5, 1–2, and 0.5–1 mg m^{-3} from top to bottom. These results will likely underestimate the NIR error that is due to the assumption that negative $[\rho_w(\lambda)]_N$ retrievals are zero in the composite-making procedure in the present version of SeaWiFS processing.

5. Discussion and Future Directions

The present study demonstrates that the black pixel assumption in ocean color remote sensing must be considered where Chl is greater than 2 mg m^{-3} . For these waters, the shape of the retrieved water-leaving reflectance spectrum is strongly altered, and Chl retrievals will be overestimated if the NIR water-leaving signal is not accounted for. However, several aspects of the NIR correction procedure are not well understood. These include the assumptions that are used to relate the NIR water-leaving reflectance to NIR inherent optical properties and the modeling of NIR inherent optical properties as a function of Chl. In the following, we address these issues and provide some thoughts about future research directions.

Many important radiative transfer processes were neglected in the present estimates of $[\rho_w(\lambda_{\text{NIR}})]_N$. These include the contributions to the water-leaving radiance because of Raman scattering, inconsistency with the bidirectional reflectance distribution function (BRDF) for NIR wave bands, and the influence of changes in the ambient ocean temperature on the present determinations of $[\rho_w(\lambda_{\text{NIR}})]_N$. These issues can be addressed by use of a radiative transfer model (Hydrolight version 4.02³¹). The inclusion of Raman scattering processes should increase the NIR water-leaving reflectance $[\rho_w(\lambda_{\text{NIR}})]_N$. We find that for Chl greater than $\sim 0.5 \text{ mg m}^{-3}$ and reasonable solar zenith angles, the error of not including Raman scattering in estimating $[\rho_w(\lambda_{\text{NIR}})]_N$ is less than 5% (results not shown). Only for oligotrophic concentrations (Chl = 0.05 mg m^{-3}) do errors approach 10%. Hence Raman scattering is not important to the modeling of $[\rho_w(\lambda_{\text{NIR}})]_N$.

Another poorly constrained factor is the BRDF. We evaluated differences in water-leaving radiance in the plane perpendicular to the solar plane for wavelengths of 443 and 765 nm under different solar illumination geometries and Chl concentrations. The antisolar plane is used to represent the scan line sampled by an ocean color imager. We find that the differences in the water-leaving radiance along the scan line normalized to the nadir-looking radiance estimate are consistent between the 443- and 765-nm wave bands (within 10% in the worst case). Furthermore, no large differences are found with changes in solar zenith angle or Chl. Hence BRDF changes are similar for the NIR wave bands as they are in the visible wave bands, and this is likely to be a minor issue in the determination of $[\rho_w(\lambda_{\text{NIR}})]_N$.

Changes in ambient seawater temperature can also affect estimates of $[\rho_w(\lambda_{\text{NIR}})]_N$ by altering the absorption coefficient for seawater. Values of $a_w(750)$ change with increasing temperature by the factor $0.0106 \text{ m}^{-1} \text{ } ^\circ\text{C}^{-1}$.³² Assuming clear-water conditions (Chl = 0), a 4% decrease in the value of $[\rho_w(750)]_N$ is expected for a $10 \text{ } ^\circ\text{C}$ increase of seawater temperature. Hence temperature-induced changes in seawater inherent optical properties

should not have a significant effect on NIR correction procedures.

The present NIR correction procedure provides significant improvements in SeaWiFS retrievals, especially for productive waters. However, the modeling of $b_{bp}(\lambda_{NIR})$ as a function of Chl is an important limitation. This parameterization is reasonable for case 1 waters where phytoplankton regulate the inherent optical properties of the ocean. However, it is questionable for turbid, coastal waters (case 2 oceans) where backscatter can originate from constituents other than phytoplankton.^{25,33} These materials include detrital biological material and abiotic particulates such as suspended sediments. For that reason, the modeling of $b_{bp}(\lambda_{NIR})$ on a closure-based basis, such as given in Eq. (7), is likely to be the long-term solution. The implementation of this approach requires an accurate development data set, and, to the best of our knowledge, these data currently do not exist.

Clearly, there are limits on the validity of the black pixel assumption. A value of Chl of 2 mg m^{-3} appears to be a good breakpoint above which NIR effects must be considered. However, the misapplication of the black pixel assumption is not the only factor causing the overcorrection of SeaWiFS water-leaving radiance spectra in the violet and blue region. More research into improving our ability to correct ocean color imagery is required.

Bob Arnone and Rick Stumpf brought the issue of the black pixel assumption to our attention, and their encouragement through this process is appreciated. Discussions and encouragement from Chuck McClain and Howard, Gordon, and Andre Morel are gratefully acknowledged as are the detailed comments from the anonymous reviewers. We thank Andrea Magnusson and Larry Harding for providing SeaWiFS imagery and field data from the Chesapeake Bay and Brian Schieber for the SIMBIOS match-up data. The authors gratefully acknowledge the support of NASA as part of the SIMBIOS and SeaWiFS science teams. The U.S. Environmental Protection Agency and the state governments bordering the Chesapeake Bay supported the chlorophyll observations presented. The SeaWiFS satellite mission is a joint venture of Orbital Sciences Corporation and NASA.

References

1. H. R. Gordon, "Atmospheric correction of ocean color imagery in the Earth Observing System era," *J. Geophys. Res.* **102**, 17,081–17,106 (1997).
2. H. R. Gordon and M. Wang, "Retrieval of water-leaving radiance and aerosol optical thickness over the oceans with SeaWiFS: a preliminary algorithm," *Appl. Opt.* **33**, 443–452 (1994).
3. H. R. Gordon, J. W. Brown, and R. H. Evans, "Exact Rayleigh scattering calculations for use with the Nimbus-7 Coastal Zone Color Scanner," *Appl. Opt.* **27**, 862–871 (1988).
4. H. R. Gordon and M. Wang, "Surface roughness considerations for atmospheric correction of ocean color sensors. 1: The Rayleigh scattering component," *Appl. Opt.* **31**, 4247–4260 (1992).
5. M. Wang, "Atmospheric correction of ocean color sensors: computing atmospheric diffuse transmittance," *Appl. Opt.* **38**, 451–455 (1999).
6. H. Yang and H. R. Gordon, "Remote sensing of ocean color: assessment of water-leaving radiance bidirectional effects on atmospheric diffuse transmittance," *Appl. Opt.* **36**, 7887–7897 (1997).
7. H. R. Gordon and M. Wang, "Influence of oceanic whitecaps on atmospheric correction of ocean-color sensor," *Appl. Opt.* **33**, 7754–7763 (1994).
8. R. Frouin, M. Schwindling, and P. Y. Deschamps, "Spectral reflectance of sea foam in the visible and near-infrared—in situ measurements and remote sensing implications," *J. Geophys. Res.* **101**, 14,361–14,371 (1996).
9. K. D. Moore, K. J. Voss, and H. R. Gordon, "Spectral reflectance of whitecaps: their contribution to water-leaving radiance," *J. Geophys. Res.* **105**, 6493–6499 (2000).
10. H. R. Gordon and D. K. Clark, "Clear water radiances for atmospheric correction of coastal zone color scanner imagery," *Appl. Opt.* **20**, 4175–4180 (1981).
11. H. R. Gordon and A. Y. Morel, *Remote Assessment of Ocean Color for Interpretation of Satellite Visible Imagery: A Review* (Springer-Verlag, New York, 1983).
12. J. E. O'Reilly, S. Maritorena, B. G. Mitchell, D. A. Siegel, K. L. Carder, S. A. Garver, M. Kahru, and C. R. McClain, "Ocean color chlorophyll algorithms for SeaWiFS," *J. Geophys. Res.* **103**, 24,937–24,953 (1998).
13. H. R. Gordon, O. B. Brown, R. H. Evans, J. W. Brown, R. C. Smith, K. S. Baker, and D. K. Clark, "A semianalytic radiance model of ocean color," *J. Geophys. Res.* **93**, 10,909–10,924 (1988).
14. S. A. Garver and D. A. Siegel, "Inherent optical property inversion of ocean color spectra and its biogeochemical interpretation: I. Time series from the Sargasso Sea," *J. Geophys. Res.* **102**, 18,607–18,625 (1997).
15. K. L. Carder, F. R. Chen, Z. P. Lee, S. K. Hawes, and D. Kamykowski, "Semianalytic Moderate-Resolution Imaging Spectrometer algorithms for chlorophyll a and absorption with bio-optical domains based on nitrate-depletion temperatures," *J. Geophys. Res.* **104**, 5403–5421 (1999).
16. C. R. McClain, M. L. Cleave, G. C. Feldman, W. W. Gregg, S. B. Hooker, and N. Kuring, "Science quality SeaWiFS data for global biosphere research," *Sea Technol.* **39**, 10–16 (1998).
17. B. D. Schieber and C. R. McClain, "L_{wN} and chlorophyll-a matchup analyses," in *SeaWiFS Postlaunch Calibration and Validation Analysis*, SeaWiFS Postlaunch Technical Report Series, NASA Tech. Memo. 1999-206892, S. B. Hooker and E. R. Firestone, eds. (NASA Goddard Space Flight Center, Greenbelt, Md., 2000).
18. R. A. Arnone, P. Martinolich, R. W. Gould, M. Sydor, and R. P. Stumpf, "Coastal optical properties using SeaWiFS," *Ocean Optics XIV Conference*, Kailua-Kona, Hawaii, 10–13 November 1998; *Ocean Optics XIV CD-ROM* (Office of Naval Research, Washington, D.C., 1998).
19. K. G. Ruddick, F. Ovidio, and M. Rijkeboer, "Atmospheric correction of SeaWiFS imagery for turbid coastal and inland waters," *Appl. Opt.* **39**, 897–912 (2000).
20. C. Hu, K. L. Carder, and F. Muller-Karger, "Atmospheric correction of SeaWiFS imagery over turbid coastal waters: a practical method," *Remote Sens. Environ.* (to be published).
21. R. W. Austin, "The remote sensing of spectral radiance from below the ocean surface," in *Optical Aspects of Oceanography*, N. G. Jerlov and E. S. Nielson, eds. (Academic, San Diego, Calif., 1974), pp. 317–344.
22. G. M. Hale and M. R. Query, "Optical constants of water in the 200-nm to 200- μm wavelength region," *Appl. Opt.* **12**, 555–563 (1973).

23. R. C. Smith and K. S. Baker, "Optical properties of the clearest natural waters," *Appl. Opt.* **20**, 177–184 (1981).
24. A. Bricaud, A. Morel, M. Babin, K. Allali, and H. Claustre, "Variations of light absorption by suspended particles with chlorophyll a concentration in oceanic (case 1) waters: analysis and implications for bio-optical models," *J. Geophys. Res.* **103**, 31,033–31,044 (1998).
25. R. W. Gould, R. A. Arnone, and P. M. Martinolich, "Spectral dependence of the scattering coefficient in case 1 and case 2 waters," *Appl. Opt.* **38**, 2377–2383 (1999).
26. A. Morel, "Optical modeling of the upper ocean in relation to its biogenous matter content (case 1 waters)," *J. Geophys. Res.* **93**, 10,749–10,768 (1988).
27. H. Loisel and A. Morel, "Light scattering and chlorophyll concentration in case 1 waters: a reexamination," *Limnol. Oceanogr.* **43**, 847–858 (1998).
28. B. C. Johnson, E. E. Early, R. E. Eplee, Jr., R. A. Barnes, and R. T. Caffrey, "The 1997 prelaunch radiometric calibration of SeaWiFS," Vol. 4 of SeaWiFS Postlaunch Technical Report Series, NASA Tech. Memo. 2000-206892, S. B. Hooker and E. R. Firestone, eds. (NASA Goddard Space Flight Center, Greenbelt, Md., 1999).
29. M. Wang, "A sensitivity study of SeaWiFS atmospheric correction algorithm: effects of spectral band variations," *Remote Sens. Environ.* **67**, 348–359 (1999).
30. S. Maritorena and J. O'Reilly, "Update on the operational SeaWiFS chlorophyll a algorithm," in *SeaWiFS Postlaunch Calibration and Validation Analyses*, Part 2, Vol. 9, SeaWiFS Postlaunch Technical Report Series, NASA Tech. Memo. 1999-206892, S. B. Hooker and E. R. Firestone, eds. (NASA Goddard Space Flight Center, Greenbelt, Md., 2000).
31. C. D. Mobley, *Hydrolight 4.0 Users Guide* (Sequoia Scientific, Inc., Mercer Island, Wash., 1998).
32. W. S. Pegau, D. Gray, and J. R. V. Zaneveld, "Absorption and attenuation of visible and near-infrared light in water: dependence on temperature and salinity," *Appl. Opt.* **36**, 6035–6046 (1997).
33. M. Sydor and R. A. Arnone, "Effect of suspended particulate and dissolved organic matter on remote sensing of coastal and riverine waters," *Appl. Opt.* **36**, 6905–6912 (1997).